Supporting Information

Puig *et al.* 10.1073/pnas.0712219105

SI Methods

Identification of FSi in VGAT-Venus Transgenic Rats *in Vivo*. In each experiment, a VGAT-Venus transgenic rat was implanted with two stimulating electrodes, one in the dorsal raphe (DR) and another in the dorsal striatum (STR). Cortico-raphe (1) (CR, $n = 24$) and crossed-corticostriatal (2) (CCS, $n = 48$) projection neurons were identified by antidromic electrical stimulation from DR and the contralateral striatum, respectively (Fig. S1*A*). We did not find any unit projecting to DR and contralateral striatum simultaneously ($n = 72$), an indication that CCS and CR pyramidal neurons may belong to different populations. Neurons with brief action potentials (<1 ms, first plus second phases, Fig. S2*A*), and no antidromic responses were considered putative FSi. At the end of the recording session, units were stained with a juxtacellular injection of neurobiotin using 500-ms cycles of positive current pulses (200 ms on/300 ms off, <8 nA) (3) (Fig. S1*B*, *Left*). Next, we examined whether there was colocalization of neurobiotin and Venus immunofluorescence. Venus-positive cells (interneurons) were further processed for PV immunoreactivity (Fig. S1*B* *Middle*).

During the positive pulses of the juxtacellular stainings, FSi were depolarized to high firing rates (>100 Hz) and often showed an increase in the amplitude of action potentials. Conversely, all of the other classes of neurons displayed much lower discharge frequencies (<50 Hz) and clear activity-dependent amplitude attenuation (Fig. S1 *B* and *C*). Most FSi could not be recovered after the staining; however, the maximum frequency induced during the depolarizing phases could be assessed. Three FSi reconstructed with Neurolucida exhibited basket cell-like morphology (4–6) (Fig. S1*B* *Right*), but other FSi could not be classified because of poor axonal labeling. Identified pyramidal neurons exhibited longer spike widths and lower discharge rates compared to FSi. However, there was some overlap in the distributions (see Fig. S2*B* and Table 1). Remarkably, 10 of 10 PV-positive cells tested emitted high-frequency bursts of action potentials when the striatum was stimulated. The short delay of the responses (≈6 ms) strongly suggested a monosynaptic activation (Fig. S1*D*). Because the striatum does not project back to cortex directly, the high discharge rate recorded during the excitations was likely caused by a feedforward activation from CCS pyramidal cells that had been antidromically activated in the striatum (Fig. S5*B*). Interestingly, five of these FSi were also excited by DR stimulation (feedforward activation from CR pyramidal neurons antidromically activated in the DR). Therefore, some FSi may receive convergent input from pyramidal neurons belonging to distinct brain circuits (Fig. S1*D*). Only 1 of 72 pyramidal cells recorded was activated by striatal stimulation, and the firing rate was much lower than that elicited in FSi (Table S1).

1. Puig MV, Artigas F, Celada P (2005) Modulation of the activity of pyramidal neurons in rat prefrontal cortex by raphe stimulation in vivo: involvement of serotonin and GABA. *Cereb Cortex* 15:1–14.
2. Morishima M, Kawaguchi Y (2006) Recurrent connection patterns of corticostriatal pyramidal cells in frontal cortex. *J Neurosci* 26:4394–4405.
3. Pinault D (1996) A novel single-cell staining procedure performed in vivo under electrophysiological control: morpho-functional features of juxtacellularly labeled thalamic cells and other central neurons with biocytin or neurobiotin. *J Neurosci Methods* 65:113–136.
4. Kawaguchi Y, Kubota Y (1993) Correlation of physiological subgroupings of nonpyramidal cells with parvalbumin- and calbindinD28k-immunoreactive neurons in layer V of rat frontal cortex. *J Neurophysiol* 70:387–396.
5. Kawaguchi Y, Kubota Y (1997) GABAergic cell subtypes and their synaptic connections in rat frontal cortex. *Cereb Cortex* 7:476–486.
6. Uematsu M *et al.* (2008) Quantitative chemical composition of cortical GABAergic neurons revealed in transgenic Venus-expressing rats. *Cereb Cortex* 18:315–330.

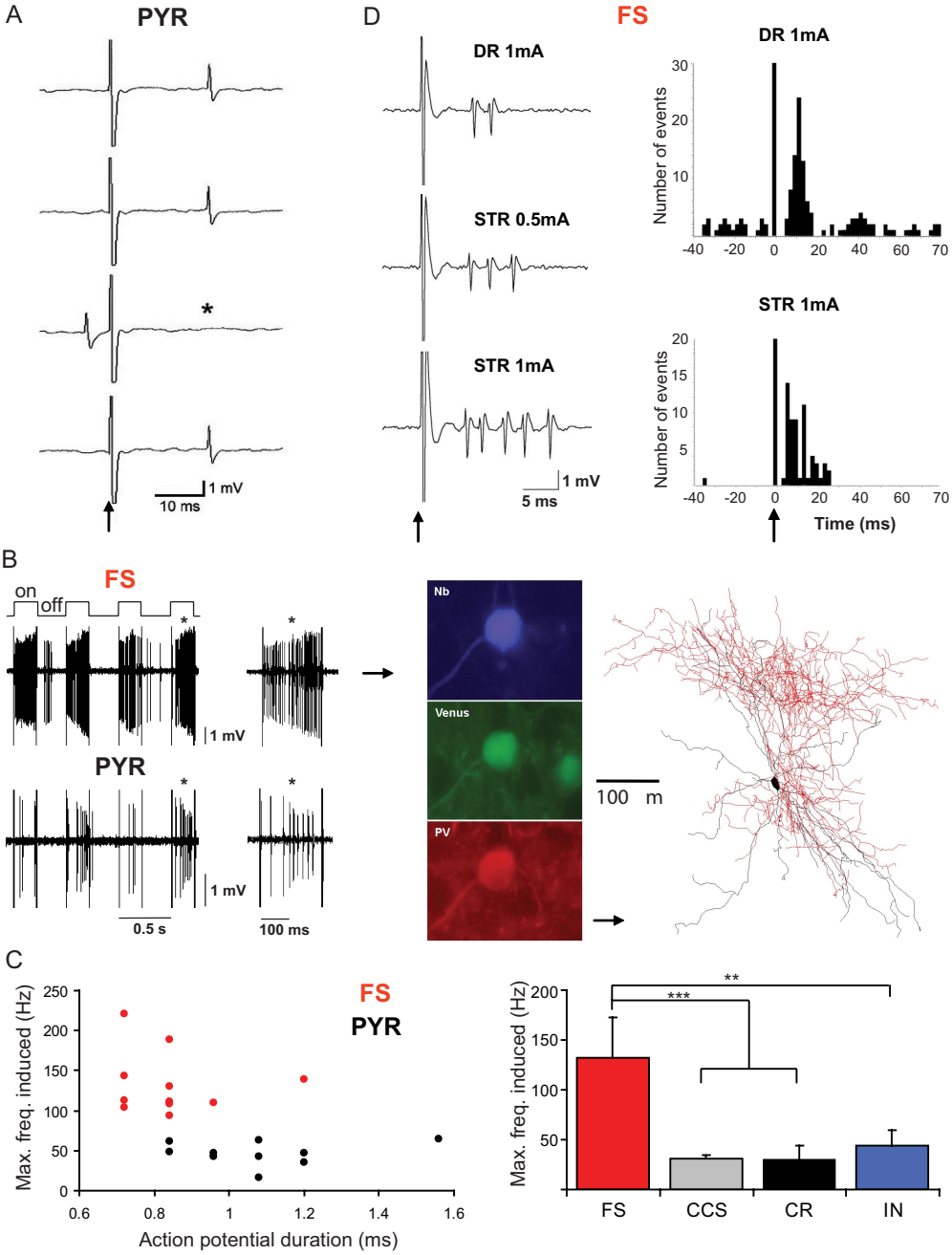

Fig. S1. *In vivo* identification of projection neurons and FSi. (*A*) Projection neurons were identified by antidromic activation. Asterisk marks a collision induced by a spontaneous occurring spike. (*B Left*) During juxtacellular injection of neurobiotin, FSi were depolarized to high firing frequencies and often exhibited an increase in the amplitude of action potentials, whereas pyramidal cells showed a marked activity dependent amplitude accommodation (asterisks). (*Center*) Labeled FSi were neurobiotin (Nb), Venus and parvalbumin (PV) positive. (*Right*) Reconstruction of a FSi with Neurolucida. Soma and dendrites are shown in black, and the axon in red. (*C Left*) We compared the maximum discharge frequency induced during staining (at the minimum current that promoted coupling of the cell, <8 nA) in 11 FSi and 10 pyramidal cells unidentified by antidromic stimulation, some of which displayed narrow action potentials. Pyramidal cells were identified morphologically by staining, and FSi by parvalbumin immunohistochemistry. Maximum frequencies were computed by averaging the firing rate of the 10 positive phases displaying the highest firing frequencies. Pyramidal cells discharged at maximum frequencies of ≈60 Hz. In contrast, 10 of 11 FSi fired above 100 Hz. (*Right*) FSi fired at significantly higher frequencies (128 ± 41 Hz, $n = 11$) than did CCS neurons (30.5 ± 4.2 Hz, $n = 7$), CR (29.6 ± 14.9 Hz, $n = 6$) and non-FSi (identified as Venus-positive PV-negative) (43.9 ± 15.5 Hz, $n = 3$) ($P < 0.001$, Kruskal–Wallis test). Bars are mean ± SD. (*D Left*) Dorsal raphe (DR) and striatal (STR) stimulations induced feedforward activations in most of the FSi recorded. The number of spikes induced depended on the stimulus amplitude. (*Right*) Peristimulus histograms were used to analyze the activations. See Table S1 for statistical analysis. Vertical arrows point to stimulus artifacts.

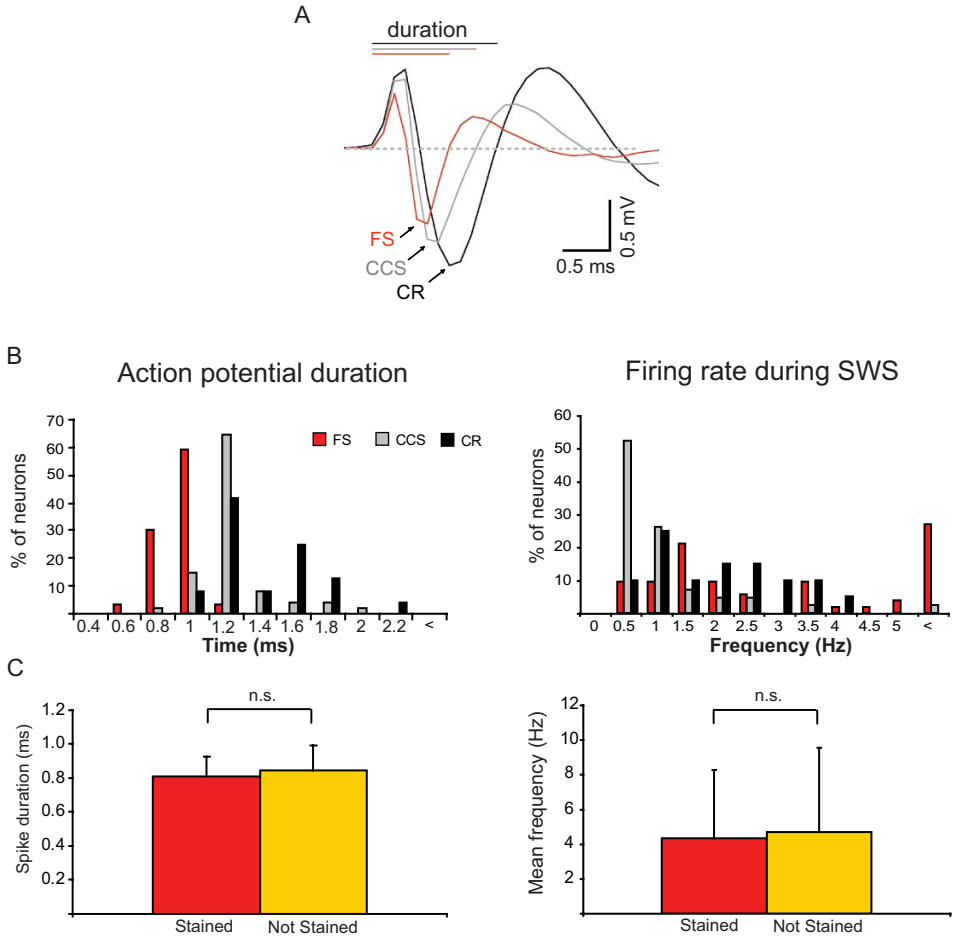

Fig. S2. Action potential duration and mean firing rate. (*A*) Representative examples of averaged action potentials (at least 10 spikes) of FSi, CR and CCS neurons. The mean action potential duration and amplitude of the three populations were significantly different. FSi had shorter waveforms and smaller amplitudes than other cell types. CR neurons had larger and more prolonged waveforms ($P < 0.001$ for both duration and amplitude, Kruskal–Wallis test). (*B*) Action potential duration and mean firing rate distributions. Most FSi displayed brief spikes (<1-ms duration). However, a small population of CCS and CR pyramidal neurons also exhibited short action potentials. In addition, CCS pyramidal cells tended to fire slower and FSi faster than the other cell subtypes, but there was an overlap between the three neuron classes. We conclude that, during SWS, the discrimination between FSi and pyramidal neurons by spontaneous discharge frequency is not possible. (*C*) Stained ($n = 13$) and unsuccessfully stained ($n = 37$) FSi displayed similar mean action potential duration and mean firing rate during SWS ($P = 0.529$ and $P = 0.845$, unpaired *t* test).

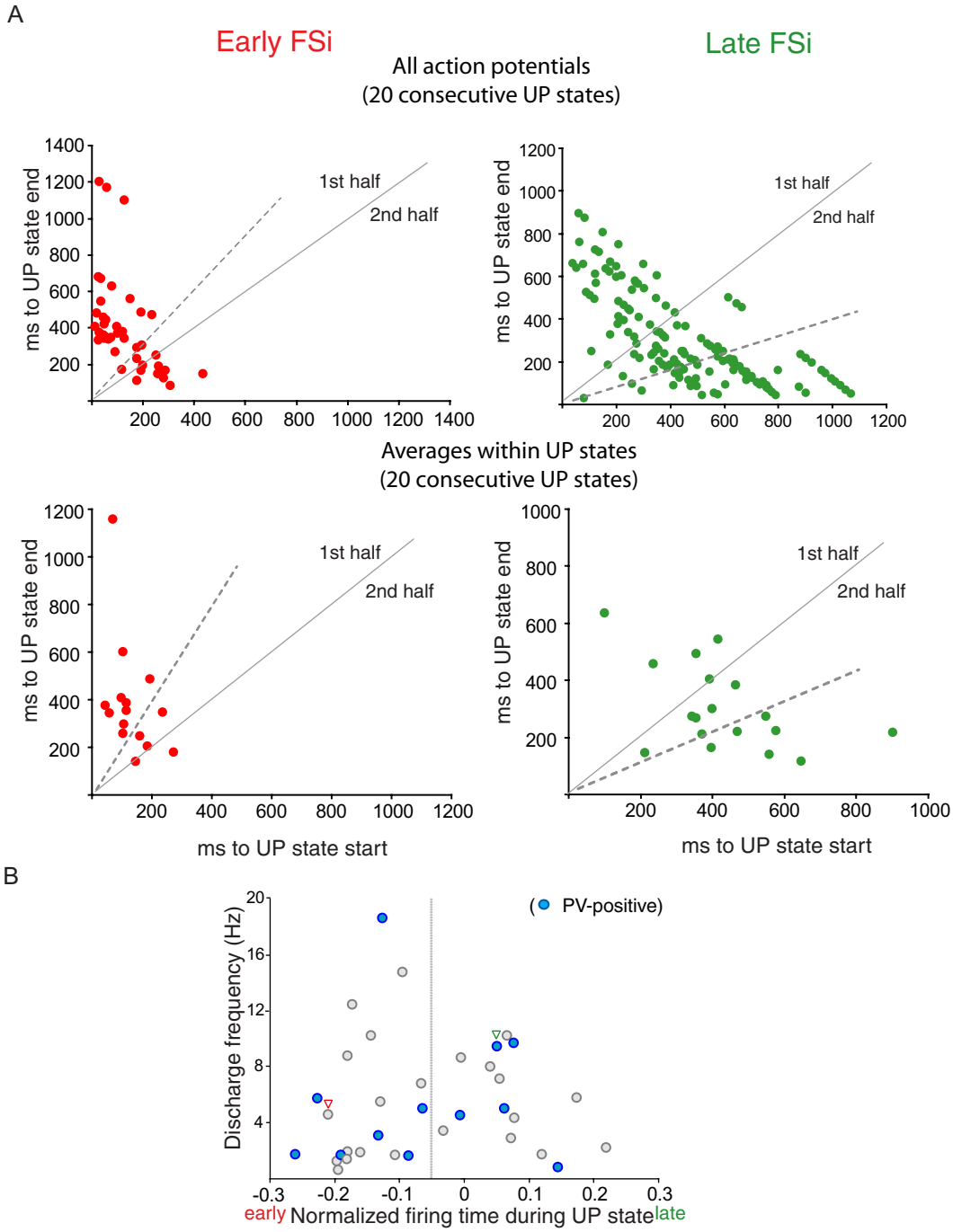

Fig. S3. Normalized UP-state time and mean firing rate. (*A*) Same early and late units of Fig. 2. (*Upper*) Time distances of all action potentials discharged during 20 consecutive UP-states with respect to start and end of UP states. Diagonals of points depict trains of action potentials. (*Lower*) Scatter plots of the averaged distances of all spikes within an UP state. Note that the late cell fires trains of action potentials all along the UP states but with a tendency to do so on the second half, as revealed by the distribution of the averages. Mean firing rate during SWS was 4.57 Hz for the early neuron and 10.21 Hz for the late neuron, and the normalized firing times were −0.21 and 0.07, respectively. Best-fit regression lines are shown. (*B*) Mean firing rate and UP-state time. Example cells in *A* have been marked. There was a general tendency for neurons firing at higher rates to display UP-state firing times closer to 0. Dotted line depicts boundary between early and late populations.

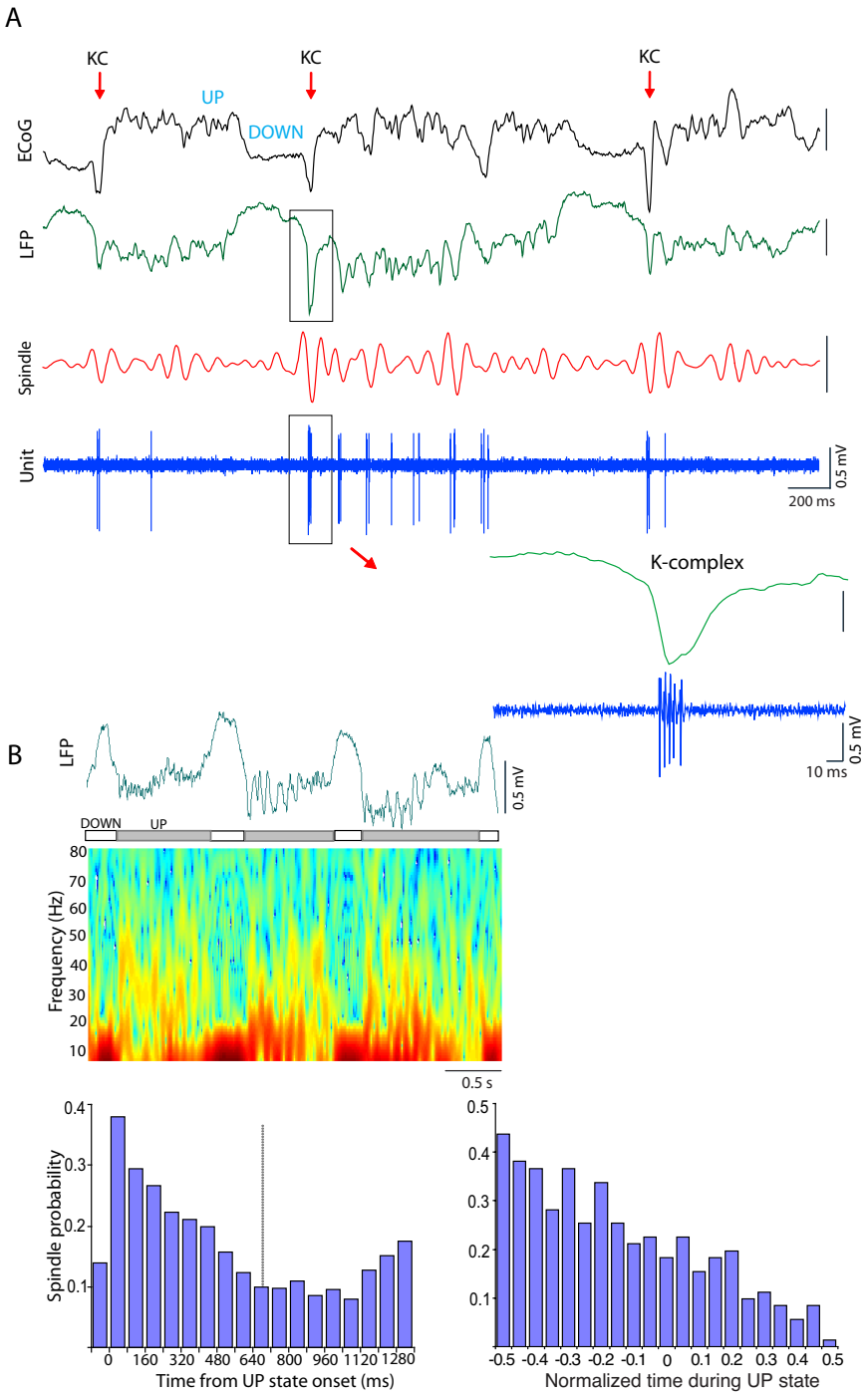

Fig. S4. (*A*) Few early FSi (3 of 50) fired in bursts, which were strongly locked to K-complexes and spindles. K-complexes occur at the beginning of UP states and consist of a sharp high-amplitude negative deflection that reflects cellular depolarization. Three consecutive UP states are shown with their corresponding K-complexes (KC). In red is the spindle band digitally filtered from the LFP. Note that the neuron fires in bursts preferentially on the first half of the UP states. Bursts were composed by at least two spikes with maximum interspike intervals of 10 ms. (*B Upper*) LFP signal and corresponding time-frequency analysis (7–80 Hz; red, maximum; blue, minimum). Spindle (7–14 Hz) and gamma (30–80 Hz) oscillations co-occur within UP states. (*Lower Left*) Spindle probability changes as UP states progress. Event histogram showing the probability of spindle trough occurrence at different times following UP-state onset. UP states were taken from 1-min epochs, aligned at the beginning of the UP state, and divided into 80-ms bins. For each bin, the probability of a spindle occurring was calculated by dividing the number of spindle troughs by the total number of UP states being analyzed. Dotted line depicts the mean UP-state duration (684 ± 181 ms, n = 8 rats). Spindle waves were present all along UP states, but there was enrichment during the first ≈150 ms and decreased occurrence at later time points. This was particularly evident for long UP states [see as examples the reduction in the spindle band power (Power Spectral Density in dBs) at the end of the second and third UP states shown in the time-frequency analysis]. (*Lower Right*) Spindle probability along UP states normalized by UP-state duration.

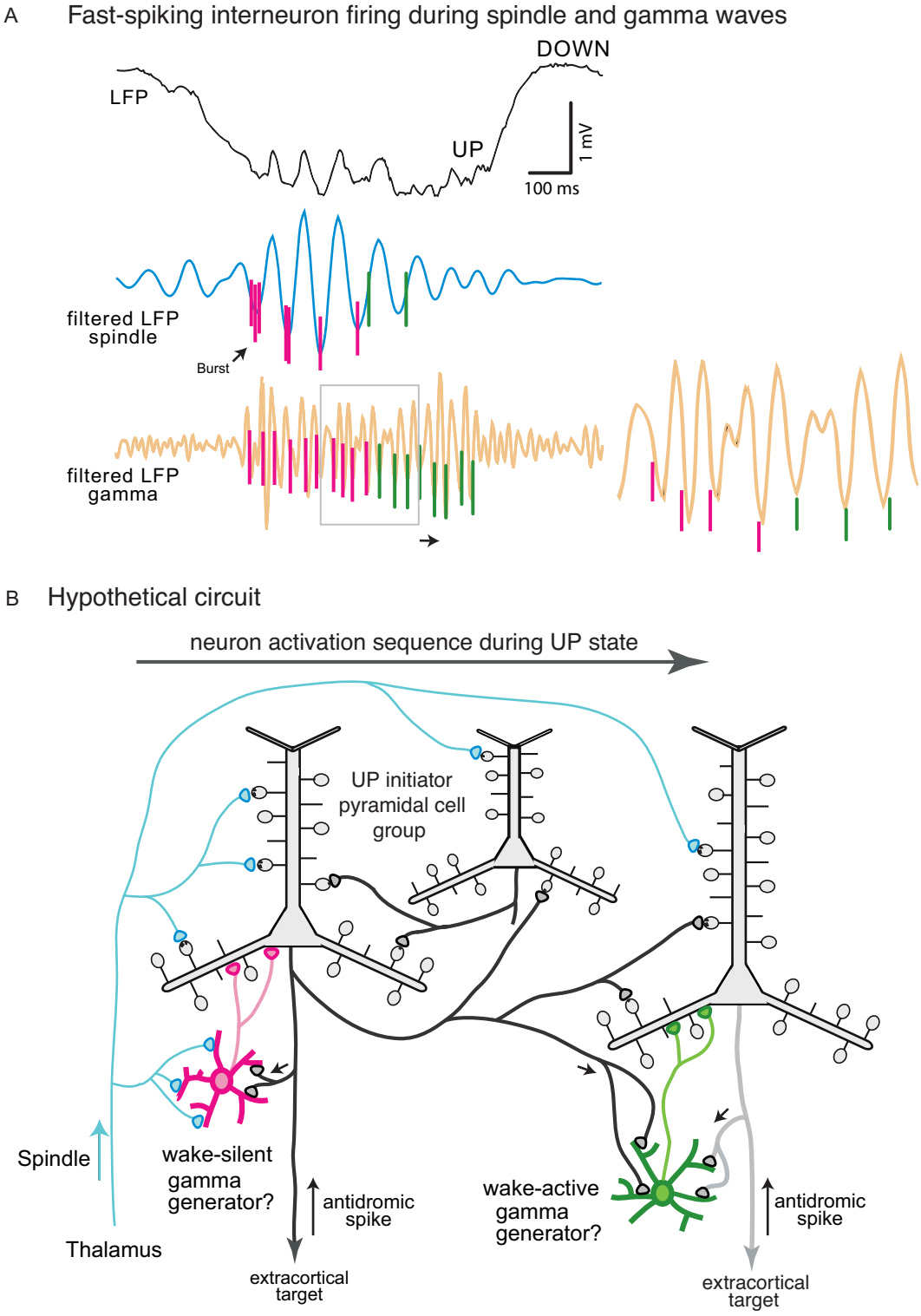

Fig. S5. Schematic summaries of the main findings. (*A*) Progressive shift in phase angles to spindle and gamma troughs between early (red) and late (green) FSi during UP states. (*B*) Hypothetical mechanism for the generation of neuronal activation sequences during UP states. Spindles synchronize early FSi and pyramidal neurons preferentially on the first half of UP states. Early FSi generate local gamma waves that recruit other units onto the ongoing network. Late FSi are local generators of gamma oscillations later within UP states.

Table S1. Differences between early and late neocortical FSi and pyramidal neurons (continues from Table 1)

	Early FSi	Late FSi	All Fsi	Pyr
STR excitation, %	77 (20/26)	87 (13/15)	81 (33/41)	1.3 (1/72)
Delay, ms	7.3 ± 4.9	4.5 ± 2.2*	6.2 ± 3.9	4
Duration, ms	10.9 ± 5.3	10 ± 5.1	10.4 ± 5.2	11
Success rate	238 ± 385	476 ± 1,376	293 ± 756	7.2
DR excitation, %	10 (3/30)	47 (7/15)	24 (11/45)	0 (0/72)
Delay, ms	4.3 ± 0.6	7.3 ± 2.4*	6.5 ± 2.3	—
Duration, ms	9 ± 2.7	14.6 ± 5.4	12.4 ± 5.1	—
Success rate	17 ± 15	18 ± 25	17.6 ± 20.6	—

Most FSi emitted high-frequency bursts of action potentials when the striatum (STR) was stimulated, whereas less FSi were activated by dorsal raphe (DR) stimulation. The majority of neurons were recorded in the secondary motor area, a region where crossed-corticostriatal (CCS) pyramidal neurons are more abundant than corticoraphe (CR) neurons. Hence, FSi recorded in the secondary motor area are more likely to receive profuse inputs from nearby CCS cells. Interestingly, more late FSi appeared to be activated by CCS and CR neurons compared to early FSi. Furthermore, the mean delay of STR excitations in late cells was significantly shorter than in early cells. This may be caused by a more abundant innervation of CCS neurons onto late FSi. *, Late vs. early, $P < 0.05$, unpaired *t* test. ( ), number of cells. Mean ± SD.